



Research on Laboratory Static Cone Penetration Test of Overlying Layer of Deep Sea Hydrate-Bearing Sediments

Shi Shen^{2*}, Rui Qin^{1,3}, Haihong Chen^{1,3}, Ting Huang^{1,3}, Yang Ge^{1,3}, Xin Lv²,
Huiyong Liang²

¹State Key Laboratory of Offshore Natural Gas Hydrates, Beijing, 100028, China

²Ningbo Institute of Dalian University of Technology, Ningbo, 315016, China

³China National Offshore Oil Corporation Research Institute Co. LTD, Beijing, 100028, China

*Corresponding Author: *Shi Shen*, shenshi_nbi@dlut.edu.cn

Abstract. The development of marine resources and deep-sea engineering construction is a crucial strategy for national security and sustainable development. However, the potential engineering geological hazards such as reservoir subsidence, wellbore instability, and submarine landslides during the extraction process necessitate precise pre-extraction analysis of reservoir characteristics. Cone Penetration Testing (CPT), an effective in-situ exploration technique, enables accurate analysis of soil types, soil layer boundaries, and physical-mechanical properties of deep-sea sediments and hydrate reservoirs by measuring penetration resistance, pore pressure changes, and other data. This study optimized the laboratory CPT testing method based on in-situ CPT tests conducted in deep-sea environments and validated it through experiments. It was found that for a 600mm-high specimen, the experimental data were most accurate when the penetration depth was between 300-400mm. An increase in the penetration rate led to an increase in both the cone tip resistance and the sidewall friction resistance. Furthermore, experiments conducted on South China Sea sediments under varying effective confining pressures demonstrated that an increase in effective confining pressure also augmented these resistance values. Based on these experimental results, this study preliminarily established empirical formulas for laboratory CPT experiments on deep-sea sediments, providing a scientific basis for reservoir safety assessments in deep-sea geotechnical engineering.

Keywords: Deep sea resources; Cone penetration test (CPT); Deep-sea geotechnical engineering; Mechanical properties; Soil classification

1 Introduction

The exploitation of marine resources deep-sea engineering construction hold significant importance for a nation's energy security and sustainable development ^[1, 2]. However, it is accompanied by risks of engineering geological hazards such as reservoir subsidence, wellbore instability, and submarine landslides^[3-5]. To ensure safe extraction, precise analysis of reservoir types, soil layer boundaries, and their physical-mechanical

© The Author(s) 2025

Y. Qiu et al. (eds.), *Proceedings of the 2024 7th International Conference on Civil Architecture, Hydropower and Engineering Management (CAHEM 2024)*, Advances in Engineering Research 256, https://doi.org/10.2991/978-94-6463-650-5_30

properties is imperative prior to exploitation [6, 7]. Cone Penetration Testing (CPT), as an efficient in-situ testing method, has been widely applied in soil investigations. Its data is invaluable in geological and geotechnical engineering for soil layer classification, soil type determination, and evaluation of engineering characteristics of foundation soils [8]. While Cone Penetration Testing (CPT) is a widely recognized in-situ testing method internationally, existing standards primarily focus on terrestrial and shallow marine environments. These standards fall short when applied to deep-sea sediments, especially in environments characterized by high pressures, complex soil structures, and unique sedimentary properties. In particular, deep-sea sediments, such as those found in the South China Sea, differ significantly from the soils typically used in developing international CPT standards. They present unique challenges such as high pore water pressure, which require specialized testing methods. Moreover, the hydrate-bearing sediments found in these environments have distinct physical and mechanical properties that cannot be accurately assessed using existing CPT interpretation techniques.

The CPT technology provides a direct basis for estimating geological parameters by penetrating a conical probe at a uniform rate and measuring the changes in cone tip resistance (q_c) and side friction resistance (f_s) with depth [9]. However, the data interpretation models and empirical formulas currently used were not designed with deep-sea conditions in mind, leading to potential inaccuracies in evaluating deep-sea sediment properties. In China, particularly in the South China Sea region, relevant testing methods and standards are still not fully developed. The lack of fitted empirical formulas creates a gap that limits the application of CPT in the study of deep-sea sediments [10]. These challenges are particularly critical in the field of deep-sea geotechnical engineering.

One of the crucial aspects in designing CPT calibration chambers is the elimination of boundary effects to ensure the accuracy of experimental results. During CPT experiments, the soil undergoes transitions through zones of disturbance, including a failure zone, plastic zone, elastic zone, and an undisturbed zone. To minimize boundary effects, it is essential to increase the ratio R_d , which is the ratio of the sample diameter to the cone diameter. Studies have shown that for loose sands, R_d should be between 20 and 50; for dense sands, R_d should be greater than 50; and when R_d exceeds 70, boundary effects are largely eliminated.

Methods to address boundary effects include increasing sample size, using special structural designs, or reducing the size of the CPT cone. While both large and small CPT calibration chambers have their advantages and disadvantages, there is currently no perfect design solution. To overcome these limitations, there is an urgent need to develop CPT standards and empirical formulas tailored to deep-sea geotechnical environments. Such developments will provide more accurate data interpretations, particularly for South China Sea sediments, and will serve as a basis for the safe and efficient exploitation of deep-sea resources and infrastructure construction.

This study aims to fill this gap by optimizing CPT testing methods, conducting laboratory CPT and triaxial experiments, and incorporating the characteristics of South China Sea sediments to establish CPT empirical formulas specific to this region. The ultimate goal is to provide scientific support for the safe and efficient exploitation of deep-sea resources and to advance deep-sea geotechnical engineering practices.

2 Test Method

2.1 Experimental Instruments

The experimental equipment used in this section is the custom-designed laboratory CPT device by the Ningbo Research Institute of Dalian University of Technology^[11], as illustrated in Figure 1. Laboratory Cone Penetration Testing is a widely accepted and commonly used testing method in geotechnical engineering, providing controlled conditions for simulating various soil environments. The device used in this study functions as a CPT chamber, a specially designed setup that allows precise testing of soil and sediment samples under laboratory conditions. The device comprises several key components: an axial loading module, a pressure control module, a temperature control module, a CPT probe, and a system program control software.

The axial loading module features a gantry-style load frame that provides stable support for the system's structure. It ensures the stability of axial loading through ball screws on both sides, enhancing the system's measurement accuracy and precise control. Moreover, it eliminates the need for manual adjustment of experimental space, making operations convenient. The system actively applies axial loads through the up-and-down movement of the loading beam, which can also lift the pressure chamber cover and body with the aid of auxiliary chains, facilitating sample loading and preparation. The pressure chamber and its upper and lower covers adopt a modular design, allowing for easy movement or replacement of various types of test chambers, such as calibration chambers, triaxial chambers, or model test chambers, via sliding rails. Additionally, the outer side of the gantry frame is equipped with a safety door for protection.

The pressure control module is responsible for regulating the confining pressure system and pore water/gas conditions. The pressure cylinder is constructed from corrosion-resistant, high-strength 316L stainless steel, capable of withstanding pressures up to 30 MPa, thereby mimicking the extreme pressure conditions of the deep sea. It incorporates four advanced pressure/volume controllers for applying confining pressure and backpressure ventilation, with a maximum working pressure of 30 MPa. These controllers are equipped with automatic pressure and volume overflow protection, ensuring a volume accuracy of 0.1% of the measured value and a pressure accuracy of 0.1% of the measurement range. Volume changes are measured and displayed with a resolution of 1 mm³. The backpressure medium can be a mixture of gases such as carbon monoxide, methane, and water. The pressure chamber adopts a cylindrical design, with its lower part bolted securely to the edge of the base and an upper lifting lug that allows for electric lifting via a mobile lifting device or the gantry frame's crossbeam. The entire chamber is made of 316L stainless steel, resistant to acid and alkali corrosion. Through an adaptive centering design for the loading connection mechanism, the system automatically aligns itself, eliminating the need for repeated adjustments.

The CPT probe features a compact design, equipped with two independent load cells, allowing for the separate and undisturbed measurement of cone tip resistance and side friction resistance. This design eliminates the need to consider friction issues related to sealing rings.



Fig. 1. Structure diagram of experimental equipment

2.2 Preparation of Test Specimens

In this study, the test samples used were marine soil (overlying layer of hydrate-bearing sediments) from the South China Sea, specifically collected by the authors during an engineering project in collaboration with China National Offshore Oil Corporation (CNOOC) on one of voyages. A series of penetration experiments were conducted on both materials under high-pressure and temperature-controlled conditions within a constructed CPT calibration tank. The particle size distribution curves of the two materials are shown in Figure 2. The specific gravity of the sand is 2.65 g/cm^3 , with a median particle diameter (d_{50}) of $60.81 \mu\text{m}$. In contrast, the specific gravity of the marine soil is 2.71 g/cm^3 , and its median particle diameter (d_{50}) is $7.27 \mu\text{m}$.

The dimensions of the test specimens were set to a diameter of 300mm and a height of 600mm . The required mass of soil samples was calculated based on the porosity requirements. The dried and crushed soil samples were weighed according to these requirements and mixed thoroughly with an appropriate amount of water. Sample preparation was carried out in a mold lined with a rubber membrane, following the relevant requirements of the layered compaction method. Equal masses of soil samples were taken and filled into the mold, which was then compacted using a tamper. The corresponding height was measured after each compaction. Once the sample preparation was completed, the specimens were placed inside a pressure chamber, as shown in Figure 3.

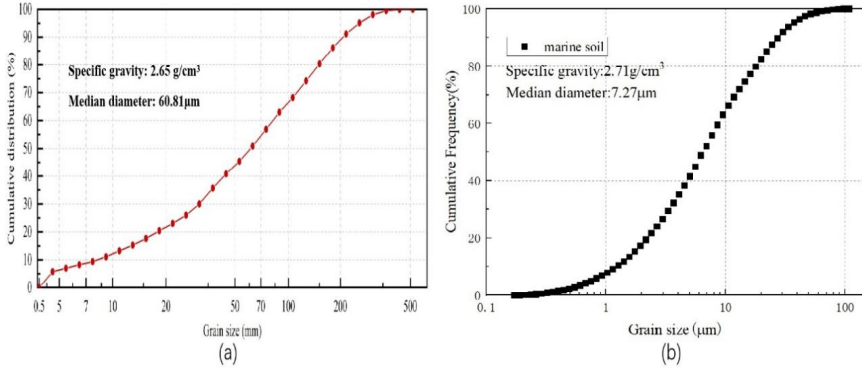


Fig. 2. Particle size distribution curve: (a) Sand soil; (b) Marine soil



Fig. 3. The sample is being loaded into the pressure chamber

2.3 Saturation of the Sample

The pressure chamber maintained a confining pressure of 0.1MPa. The temperature inside the chamber was adjusted to the target temperature T , and the pore pressure within the sample was increased to P . Simultaneously, the confining pressure was increased at the same rate to $(P + 0.1)$. The inlet pressure (P) and confining pressure ($P + 0.1$) of the sample remained constant, while the outlet pressure of the sample was adjusted to P_1 ($P_1 = P - 0.2$) using a back-pressure valve. To verify if the sample had achieved water saturation, ultrapure water with a temperature of T and a pressure of P was injected into the inlet of the sample using a back-pressure controller. The B-value

was measured through the back-pressure saturation method. The criterion for saturation was based on calculating the pore pressure coefficient B using Skempton's formula:

$$B = \Delta u / \Delta \sigma_3 \quad (1)$$

In the formula,

$\Delta \sigma_3$ —the increase in confining pressure;

Δu —the increase in pore pressure caused by the increase in confining pressure.

2.4 Sample Consolidation

After the water saturation process of the sample is completed, the confining pressure σ'_c acting on the sample is determined based on the effective confining pressure $\sigma_c (\sigma_c = \sigma'_c + P_2)$. The pore pressure of the sample is adjusted to P_2 using a high-pressure plunger pump, and the confining pressure is increased at the same rate, ensuring that the effective confining pressure on the sample remains σ'_c throughout. The temperature of the sample is then adjusted to T_1 using a low-temperature circulating water bath, while maintaining constant pore pressure and confining pressure during this process. Next, the confining pressure of the sample is adjusted to σ'_c to initiate the consolidation process, allowing the fluid within the sample to slowly drain out and the excess pore water pressure to gradually dissipate. When more than 95% of the excess pore water pressure has dissipated, the consolidation process is considered complete.

2.5 Sample Penetration

After the consolidation process is completed, an indoor cone penetration test (CPT) is conducted. The CPT probe is penetrated into the sample at a constant rate, and the cone tip resistance, side friction resistance, and pore pressure of the experimental sample are recorded.

2.6 data Processing

Cone tip resistance

$$q_c = Q_c / A_c \quad (2)$$

Include: q_c represents cone tip resistance, MPa

Q_c represents the measured cone force, KN

A_c represents the cross-sectional area behind the cone tip

Friction resistance

$$f_s = Q_s / A_s \quad (3)$$

Include: f_s represents the frictional resistance of the sidewall, MPa

Q_s represents the force on the friction sleeve, KN

A_s represents the surface area of the friction sleeve.

3 Results and Discussion

3.1 Indoor Penetration Test on Sandy Soil

This section conducted indoor static penetration tests on sandy soil using penetration rates of 0.1mm/s, 0.5mm/s, and 1mm/s, and the specific experimental conditions are shown in Table 1. The experimental results and analysis are as follows:

Table 1. Experimental conditions and parameters

Effective confining pressure (MPa)	porosity (%)	Penetration rate (mm/s)	Temperature (°C)
1.0	50	0.1	5
1.0	50	0.5	5
1.0	50	1.0	5

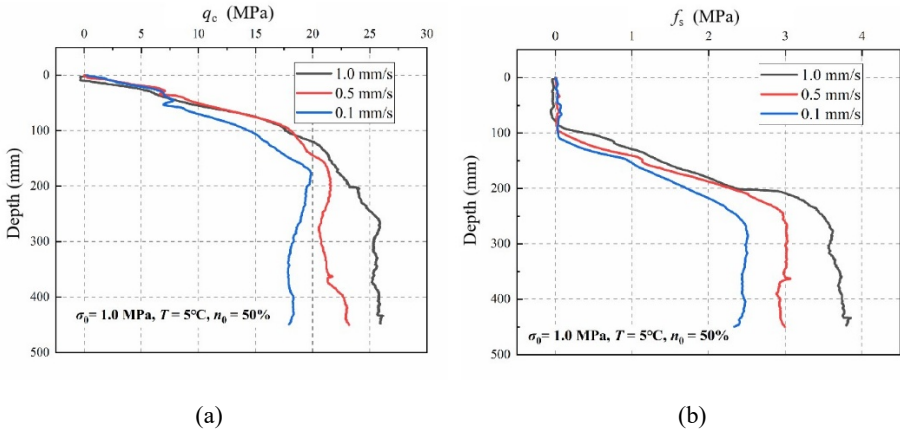


Fig. 4. Experimental results at different penetration rates: (a) Comparison of cone tip resistance; (b) Comparison of frictional resistance

As evident from Figure 4-a, under an effective confining pressure of 1MPa, the cone tip resistance curves for three different penetration rates exhibit similar trends, which can be divided into two stages: (1) an initial stage of continuous increase during the early penetration, and (2) a relatively stable stage during the middle to late penetration. As the strain rate increases, the entire curve shifts to the right. Figure 4-b shows that under an effective confining pressure of 1MPa, the trends of the side friction resistance curves for different penetration rates can be divided into three stages: (1) an initial stage where the value is zero during the initial penetration, (2) a stage of continuous increase in side friction resistance as the friction sleeve fully contacts the soil sample, and (3) a stable stage during the middle to late penetration. Based on the experimental results, the relationship between the average cone tip resistance during the 300-400mm pene-

tration stage and the penetration rate can be fitted as shown in Figure 5. It can be observed from the figure that an increase in the strain rate leads to an increase in the cone tip resistance value.

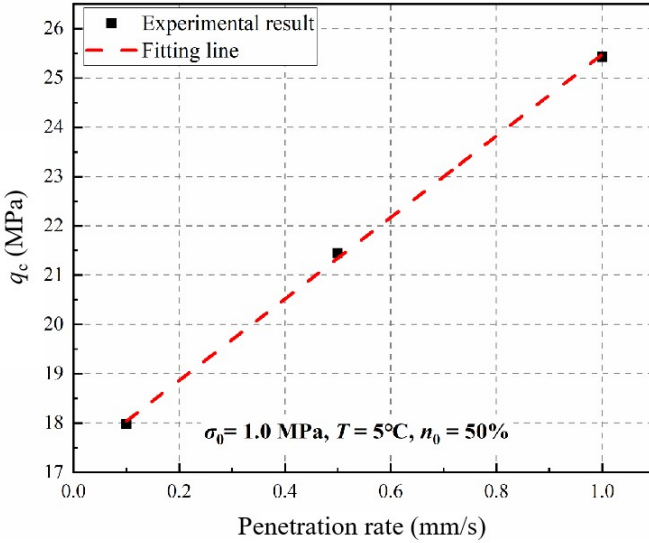


Fig. 5. The relationship between cone tip resistance and penetration rate

3.2 South China Sea Muddy Silt

Indoor Static Penetration Test. The main purpose of this section is to preliminarily establish the correlation between indoor static cone penetration tests and triaxial tests of South China Sea sediments. The specific experimental conditions are shown in the table.

Table 2. Experimental Conditions and Parameters

Effective confining pressure (MPa)	Porosity (%)	Penetration rate (mm/s)	Temperature (°C)
0.5	45	0.1	5
1.0	45	0.1	5
1.5	45	0.1	5

Based on Equation (2), the obtained cone tip resistance data were processed and plotted in Figure 6 to illustrate the trends of cone tip resistance under different effective confining pressures. The trends observed under different effective confining pressures are similar, with both showing two distinct stages: (1) an initial stage of increase during the early penetration, and (2) a stable stage during the middle to late penetration. Additionally, as the effective confining pressure increases, the entire curve shifts to the right.

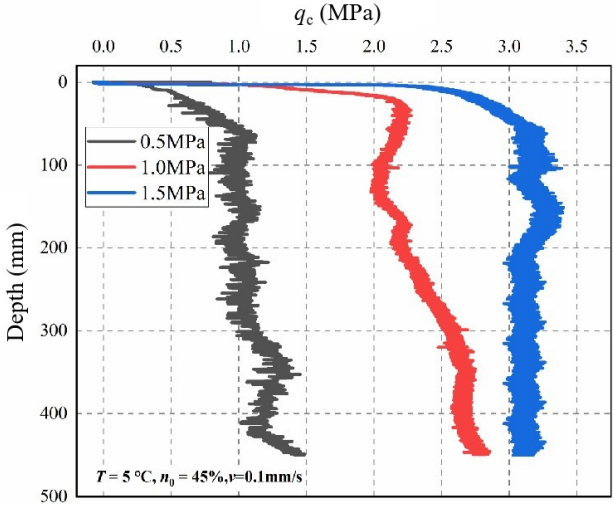


Fig. 6. The change of cone resistance with penetration depth under different effective confining pressures

By selecting the average cone tip resistance values from the experimental results within the penetration depth range of 300mm-400mm, a relevant relationship can be plotted as shown in the following figure. According to Figure 7, it can be observed that as the effective confining pressure increases, the cone tip resistance value also increases. The primary reason for this is that an increase in effective confining pressure leads to a tighter arrangement of particles within the sample, resulting in a stronger resistance to external forces^[12]. This observation is consistent with the effect of effective confining pressure on soil strength^[13, 14].

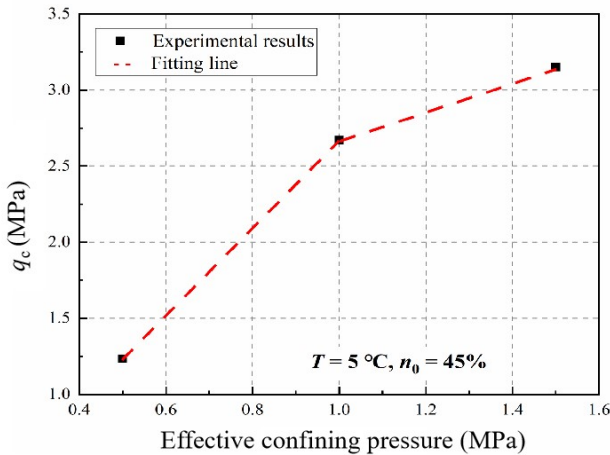


Fig. 7. Relationship between effective confining pressure and cone resistance

Triaxial Test. The figure 8 depicts the relationship between deviatoric stress and axial strain during a triaxial undrained shear test under varying effective confining pressures. At low effective confining pressures, the deviatoric stress initially increases and then decreases as the axial strain increases, indicating the presence of strain softening behavior. However, at a specific condition of 2MPa effective confining pressure, the deviatoric stress continues to increase with increasing axial strain, exhibiting strain hardening. Furthermore, it is observable that as the effective confining pressure increases, the maximum deviatoric stress that the sample can withstand also increases. This indicates that with higher effective confining pressures, the failure strength of the test specimen becomes greater.

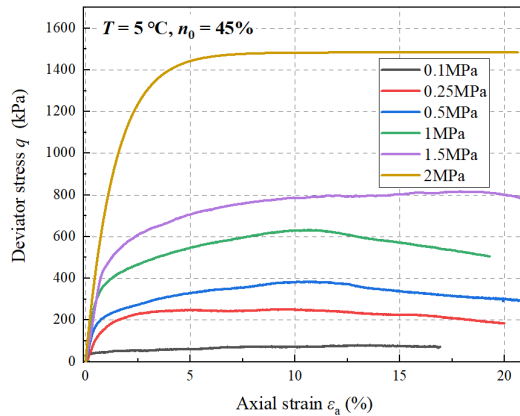


Fig. 8. The change of deviator stress with effective confining pressure under different effective confining pressures

The Correlation between Static Cone Penetration Test and Triaxial Test.

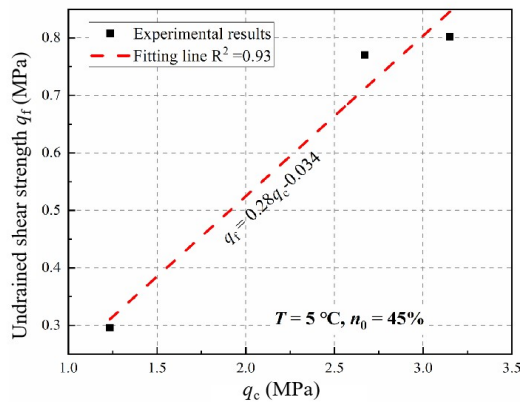


Fig. 9. Relationship between undrained shear strength and cone tip resistance

Based on the relationship between cone tip resistance and effective confining pressure in static penetration tests, as well as the relationship between undrained shear strength and effective confining pressure in triaxial tests, the relationship between undrained shear strength and cone tip resistance can be obtained as shown in Fig. 9. The empirical relationship between undrained shear strength and cone tip resistance was obtained as follows:

$$q_f = 0.28q_c - 0.034$$

4 Conclusions

The present study addresses the challenges of interpreting in-situ Cone Penetration Test (CPT) data in deep-sea environments by optimizing laboratory CPT testing methods for deep-sea sediments based on experimental data. Laboratory CPT tests and triaxial mechanical property tests were conducted, leading to the preliminary establishment of a formula model linking cone tip resistance and undrained shear strength. The specific conclusions are as follows:

1. For sandy soil tests under an effective confining pressure of 1 MPa, the study confirmed that both cone tip resistance and side friction resistance increase as penetration rate rises, indicating a strong correlation between penetration rate and the soil's mechanical behavior. This behavior was observed in two distinct stages: an initial increase followed by stabilization.

2. For marine soils, the experimental results highlighted that cone tip resistance and side friction resistance similarly exhibit two stages of increase and stabilization, with higher effective confining pressures consistently leading to higher resistance values. These results underscore the importance of confining pressure in evaluating deep-sea sediment properties.

3. One of the most important contributions of this study is the development of an empirical formula linking CPT cone tip resistance to undrained shear strength for sediments overlying hydrate reservoirs. This formula serves as a valuable tool for future research and practical applications in deep-sea geotechnical engineering.

Acknowledgements

This study was supported by the State Key Laboratory of Offshore Natural Gas Hydrates (2022-KFJJ-SHW), the Natural Science Foundation of Ningbo (2022J005), Grants from the Beijing New-star Plan of Science and Technology (NO.20240484721).

References

1. Ma, S., Liu, Z., Zheng, J.-N., Wu, Z., Li, N., Guan, X., Han, J.-N., Yang, M. & Song, Y. (2024) Natural Gas Hydrate Decomposition Characteristics at the Exploitation Anaphase via

- Sediment Warming. *Energy & Fuels*, 38: 14334-14342. <http://doi.org/10.1021/acs.energyfuels.4c02709>.
2. Chen, B., Sun, H., Li, K., Yu, T., Jiang, L., Yang, M. & Song, Y. (2023) Unsaturated water flow-induced the structure variation of gas hydrate reservoir and its effect on fluid migration and gas production. *Energy*, 282: 128843. <http://doi.org/10.1016/j.energy.2023.128843>.
 3. Wang, L., Shen, S., Wu, Z., Wu, D. & Li, Y. 2024. Strength and creep characteristics of methane hydrate-bearing clayey silts of the South China Sea. *Energy*, 294: 130789. <http://doi.org/10.1016/j.energy.2024.130789>.
 4. Wang, L., Li, Y., Shen, S., Liu, W., Sun, X., Liu, Y. & Zhao, J. (2022) Mechanical behaviours of gas-hydrate-bearing clayey sediments of the South China Sea. *Environmental Geotechnics*, 9: 210-222. <http://doi.org/10.1680/jenge.19.00048>.
 5. Sun, H., Chen, J., Ji, X., Karunakaran, G., Chen, B., Ranjith, P. G., Song, Y. & Yang, M. (2024) Optimizing CO₂ hydrate storage: Dynamics and stability of hydrate caps in submarine sediments. *Applied Energy*, 376: 124309. <http://doi.org/10.1016/j.apenergy.2024.124309>.
 6. Wang, L., Li, Y., Wu, P., Shen, S., Liu, T., Leng, S., Chang, Y. & Zhao, J. (2020) Physical and mechanical properties of the overburden layer on gas hydrate-bearing sediments of the South China sea. *Journal of Petroleum Science and Engineering*, 189: 107020. <http://doi.org/10.1016/j.petrol.2020.107020>.
 7. Wang, L., Sun, X., Shen, S., Wu, P., Liu, T., Liu, W., Zhao, J. & Li, Y. (2021) Undrained triaxial tests on water-saturated methane hydrate-bearing clayey-silty sediments of the South China Sea. *Canadian Geotechnical Journal*, 58: 351-366. <http://doi.org/10.1139/cgj-2019-0711>.
 8. Wu, Z., Gu, Q., Wang, L., Li, G., Shi, C., He, Y., Li, Q. & Li, Y. (2024) Experimental Study on Permeability and Gas Production Characteristics of Montmorillonite Hydrate Sediments Considering the Effective Stress and Gas Slippage Effect. *SPE Journal*, 29: 2525-2544. <http://doi.org/10.2118/218385-PA>.
 9. Ayala, J., Fourie, A. & Reid, D. (2020) Cone penetration testing on silty tailings using a new small calibration chamber. *Géotechnique Letters*, 10: 492-497. <http://doi.org/10.1680/jgele.20.00037>.
 10. Li, Y., Hu, G., Wu, N., Liu, C., Chen, Q. & Li, C. A. (2019) Undrained shear strength evaluation for hydrate-bearing sediment overlying strata in the Shenhu area, northern South China Sea. *Acta Oceanologica Sinica*, 38: 114-123. <http://doi.org/10.1007/s13131-019-1404-8>.
 11. Ge, Y., Wang, L., Feng, K., Shen, S., Liu, Y., Wu, Z., Liu, Z. & Song, Y. (2024) High-pressure and temperature-controlled CPT calibration chamber based on deep-sea hydrate reservoirs. *Geoenergy Science and Engineering*, 242: 213207. <http://doi.org/10.1016/j.geoen.2024.213207>.
 12. Wang, L., Shen, S., Wu, Z., Wu, D. & Li, Y. 2024. Strength and creep characteristics of methane hydrate-bearing clayey silts of the South China Sea. *Energy*, 294: 130789. <http://doi.org/10.1016/j.energy.2024.130789>.
 13. Wang, L., Yu, W., Ge, Y., Shen, S., Wu, Z., Zhu, Y., Song, Y. & Li, Y. (2024) Undrained triaxial tests of underconsolidated overlying sediments of hydrate deposits in the South China Sea. *Gas Science and Engineering*, 131: 205442. <http://doi.org/10.1016/j.gjsce.2024.205442>.
 14. Liu, W., Liu, H., Wang, L., Feng, K., Shen, S., Liu, Y., Zhao, J. & Li, Y. (2024) Undrained Mechanical Properties of Overlying Soils of Gas Hydrate Reservoirs in the South China Sea. *Energy & Fuels*, 38: 3020-3031. <http://doi.org/10.1021/acs.energyfuels.3c04389>.

Open Access This chapter is licensed under the terms of the Creative Commons Attribution-NonCommercial 4.0 International License (<http://creativecommons.org/licenses/by-nc/4.0/>), which permits any noncommercial use, sharing, adaptation, distribution and reproduction in any medium or format, as long as you give appropriate credit to the original author(s) and the source, provide a link to the Creative Commons license and indicate if changes were made.

The images or other third party material in this chapter are included in the chapter's Creative Commons license, unless indicated otherwise in a credit line to the material. If material is not included in the chapter's Creative Commons license and your intended use is not permitted by statutory regulation or exceeds the permitted use, you will need to obtain permission directly from the copyright holder.

